The influence of chromosome density variations on the increase in nuclear disorder strength in carcinogenesis

2011 Phys. Biol. 8 015004

(http://iopscience.iop.org/1478-3975/8/1/015004)

Phys. Biol. **8** (2011) 015004 (6pp) doi:10.1088/1478-3975/8/1/015004

The influence of chromosome density variations on the increase in nuclear disorder strength in carcinogenesis

Jun Soo Kim, Prabhakar Pradhan, Vadim Backman[1] and Igal Szleifer[1]

Department of Biomedical Engineering and Chemistry of Life Processes Institute, Northwestern University, Evanston, IL 60208, USA

E-mail: v-backman@northwestern.edu and igalsz@northwestern.edu

Received 13 August 2010
Accepted for publication 27 September 2010
Published 7 February 2011
Online at stacks.iop.org/PhysBio/8/015004

Abstract

Microscopic structural changes have long been observed in cancer cells and used as a marker in cancer diagnosis. Recent development of an optical technique, partial-wave spectroscopy (PWS), enabled more sensitive detection of nanoscale structural changes in early carcinogenesis in terms of the disorder strength related to density variations. These nanoscale alterations precede the well-known microscopic morphological changes. We investigate the influence of nuclear density variations due to chromosome condensation on changes of disorder strength by computer simulations of model chromosomes. Nuclear configurations with different degrees of chromosome condensation are realized from simulations of decondensing chromosomes and the disorder strength is calculated for these nuclear configurations. We found that the disorder strength increases significantly for configurations with slightly more condensed chromosomes. Coupled with PWS measurements, the simulation results suggest that the chromosome condensation and the resulting spatial density inhomogeneity may represent one of the earliest events in carcinogenesis.

1. Introduction

Structural changes such as heterochromatin aggregation and chromosome organization are indicated in most cancer cells and used as a marker in cancer diagnosis [1, 2]. The changes are more prominent in later stages of carcinogenesis and are usually detected by conventional histological methods. Detection of the structural changes at the nanoscale, however, has been limited by the resolution of light microscopy and, therefore, has been difficult especially in early stages of carcinogenesis. The recent development of an optical technique, partial-wave spectroscopy (PWS), enabled more sensitive detection of structural changes occurring in early to late stages of carcinogenesis and has shown a potential for early diagnosis of cancer in the near future [3, 4]. PWS measures a statistical property L_d, which is defined as the product of average density fluctuations and its correlation length. Throughout this work the property L_d is termed the disorder strength following previous work [3]. Statistical averages of the disorder strength over cells show differences between normal cells and cancer cells in early stages even when they are indistinguishable by conventional histological methods. So far, the diagnostic success of the PWS has been proven for several types of cancer, including colon, pancreatic and lung cancers [3, 4].

In order to provide biological understanding of structural alterations in carcinogenesis, efforts are being made to identify structural entities and processes that are responsible for the alteration of the disorder strength, as observed in PWS measurements. For cell lines studied in the previous work a significant change in the disorder strength is observed largely in a cell nucleus [3] and analysis and quantification of their transmission electron microscopy (TEM) images showed that mass density fluctuations correlate with a degree of carcinogenesis in the cell nucleus [5]. Furthermore, it is evident that there occur nuclear density variations such as heterochromatin aggregation in many forms of cancer, as

[1] Authors to whom any correspondence should be addressed.

observed by conventional histological methods in late stages of carcinogenesis [1]. Therefore, it is reasonable to hypothesize that changes in nuclear density variations and its correlation, by chromosome structural changes, give rise to a change in disorder strength at the nuclear part of the cell.

In this work we aim to confirm the above hypothesis and investigate how nuclear density variations, especially by chromosome condensation, influence the disorder strength in a cell nucleus by computer simulations of model chromosomes. For this purpose we construct a model system composed of chromosomes with different degrees of condensation and calculate its disorder strength. The structure of chromosomes has been investigated extensively in recent years by experimental techniques such as fluorescence *in situ* hybridization (FISH) [6–8], and chromosome conformation capture (3C) and other 3C-based techniques [9–11]. These techniques showed that chromosomes occupy distinct territories and are distributed non-randomly in a cell nucleus [7–13]. Detailed understanding of chromosome structure, however, remains elusive. Furthermore, the mechanism of chromosome condensation is not clear and, therefore, the construction of a model nucleus with different chromosome condensation is not straightforward.

In order to construct a model nucleus with different degrees of chromosome condensation by compacting the constituent chromosomes, additional attractions need to be assumed between chromosome segments in an arbitrary way due to the lack of our understanding of the mechanisms responsible for chromosome condensation. In this work, we circumvent this difficulty by adopting chromosome configurations generated during decondensation of compact chromosomes. We simulate the decondensation of highly compact chromosomes driven by polymer conformational entropy and excluded volume interactions between chromosome segments. We assume that a model nucleus with chromosome configurations generated at different times of decondensation will have similar density distributions to those of a biological cell nucleus that consists of chromosomes with different degrees of condensation induced by carcinogenesis. We calculate how the condensed configurations of chromosomes alter average density variations, and density–density correlation length and thus disorder strength.

Several models of a chromosome have been proposed that can reproduce currently available experimental data: the multi-loop subcompartment model [14], the random loop model [15] and the decondensing linear polymer model [16] for the mean square intrachromosome distances measured with FISH experiments; the crumpled globule model [11, 17] for the contact probabilities with 3C-based techniques and the kinkable chromatin fiber model [18] for both properties. While the other models may be as successful in simulations of decondensation, we employ the decondensing linear polymer model in this work since the decondensation of compact chromosomes has been well studied previously for this model [16].

The rest of this paper is organized as follows: interpretation of a disorder strength measured in PWS is described in section 2, simulation model and methods are described in section 3 and also in section 4 results are presented and discussed. Finally, a summary and conclusion are presented in section 5.

2. Partial-wave (optical) spectroscopy measures the changes in nanoscale disorder strength in cells in carcinogenesis

Visible-light microscopy is the means for detection of morphological changes in cells and is restricted to the micron and supramicron scales due to the diffraction-limited resolution. Thus, efforts to understand biological processes at the nanoscale have been stymied by the lack of practical means of analysis of cellular nanoscale architecture.

Recently developed PWS enables us to image and quantify nanoscale intracellular refractive index fluctuations in terms of its disorder strength, $L_d = \langle \Delta n^2 \rangle \times l_c$, where Δn is the local fluctuating part of the intracellular refractive index which depends on the local concentration of cell solids, (e.g., chromosomes, etc) and l_c is its correlation length which depends on the size of the intracellular solids. In order to assess the nanoscale density fluctuations, PWS utilized a fundamental principle of mesoscopic light transport theory that the signal in 1D arising due to the multiple interferences of light waves reflected from weak refractive index fluctuations is sensitive to any length scale of refractive index fluctuations (for details see [3, 4]). Because an optical refractive index is a linear function of the local density of intracellular solids (proteins, lipids, DNA, RNA, etc), the spectrum of a 1D scattering signal contains information about spatial variations of density at length scales that are well below the wavelength. PWS results have shown that under realistic experimental conditions the limit of sensitivity of PWS to l_c is under 20 nm to any higher length scales [3].

It has been shown that the optical refractive index (n) is linearly proportional to the local mass density (ρ) of intracellular macromolecules such as proteins, lipids, DNA and RNA, i.e. $n = n_0 + \Delta n = n_0 + \alpha \Delta \rho$, where n_0 is the refractive index of the medium surrounding a scattering structure, ρ is the local density of solids and α is a proportionality constant which is approximately the same $\alpha \sim 0.18$ for majority of the scattering substances found in living cells [19, 20]. The above relationship provides a direct link between the mass density fluctuations in a cell and the corresponding refractive index fluctuations. Therefore, quantification of the mass density fluctuations implies the quantification of the refractive index fluctuations or the optical properties. Therefore, we can write $\Delta n = \alpha \Delta \rho$ and thus the disorder strength can be defined as

$$L_d \propto \langle \Delta \rho^2 \rangle \times l_c, \tag{1}$$

where $\Delta \rho$ is the local density variation and l_c is its correlation length.

3. Simulation model and methods

Chromosomes in a cell nucleus are modeled as a decondensing linear polymer. A similar model was employed to study

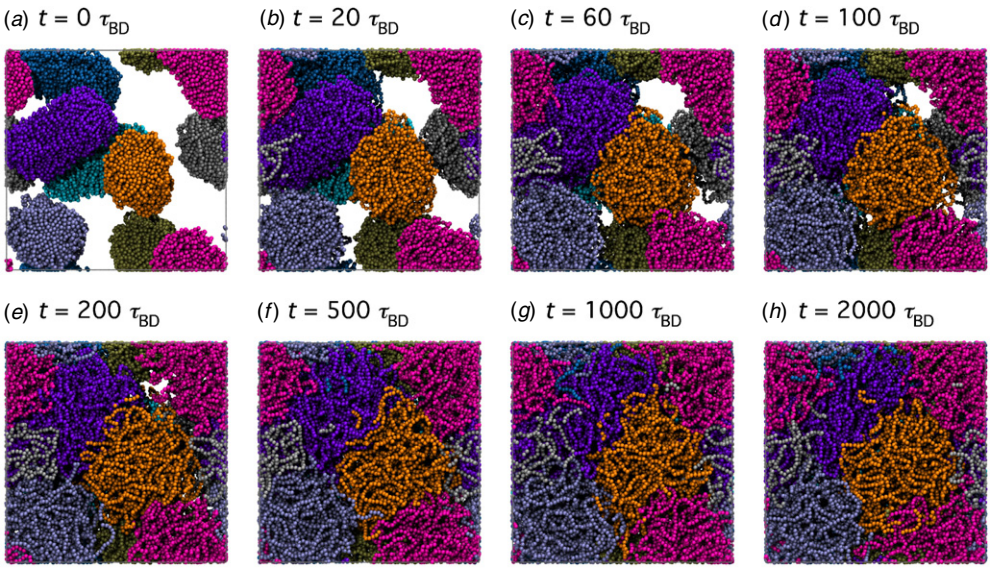

Figure 1. A set of snapshots of model chromosomes during the course of decondensation, created using VMD [25]. Eight chromosomes of ∼10 Mbp, each represented by a different color, are located in a cubic simulation box with a length of 1.6 μm, and τ_{BD} is the unit of time in Brownian dynamics simulations.

the chromosome decondensation and organization in the interphase nucleus recently by Rosa and Everaers [16]. Each model chromosome consists of 3400 segments with a diameter of 30 nm, mimicking the chromatin fiber with a thickness of 30 nm at physiological salt concentrations [21]. Each segment represents ∼3 kbp of DNA in chromatin and, therefore, each chromosome has DNA contents of ∼10 Mbp. A symbol σ represents the segment diameter of 30 nm and is used as a unit of length in this work.

Initially, eight compact chromosomes are located in a cubic simulation box with a length of ∼1.6 μm (equivalent to 52.2σ). As Brownian dynamics (BD) simulations start, the compact chromosomes decondense, mimicking the chromosome decondensation during interphase. Nuclear configurations at different times during the course of decondensation are saved, for which density variations and disorder strength are calculated. The statistical properties are calculated by averaging over 20 different realizations obtained from simulations starting from 20 independent initial configurations. The system is evolved using conventional BD [22] without hydrodynamic interactions using GROMACS version 4.0.5 with a use of tabulated interaction functions [23]. At each time step Δt, the position $\mathbf{r}_i(t)$ of a particle i is updated via

$$\mathbf{r}_i(t+\Delta t) = \mathbf{r}_i(t) + \frac{D_0 \mathbf{F}_i(t)}{k_B T}\Delta t + \mathbf{R}_i(\Delta t), \tag{2}$$

where $\mathbf{F}_i(t)$ is the total force acting on the particle i, and $\mathbf{R}_i(\Delta t)$ is a random displacement with a Gaussian distribution function with zero mean and variance–covariance $\langle \mathbf{R}_i(\Delta t)\mathbf{R}_j(\Delta t)\rangle = 2D_{0\Delta} t\delta_{ij}$. D_0 is the diffusion coefficient of the chromosome segment in pure solvent and sets the time scale by a definition of the unit of time $\tau_{\mathrm{BD}} = \sigma^2/D_0$. A time step $\Delta t = 10^{-4}\ \tau_{\mathrm{BD}}$ is used for all the simulations. A total of 2×10^8 time steps ($2 \times 10^4\ \tau_{\mathrm{BD}}$) are run for each of 20 simulations. The total force $\mathbf{F}_i(t)$ is given by the gradient of U_{total}, where U_{total} is the sum of bonded and non-bonded interactions described below.

Each chromosome segment interacts with other segments by repulsive Lennard–Jones potential of the form

$$U_{\mathrm{r}}(r) = \begin{cases} 4\varepsilon\left[\left(\frac{\sigma}{r}\right)^{12} - \left(\frac{\sigma}{r}\right)^{6}\right] + \varepsilon & 0 < r < r_{\mathrm{c}} \\ 0 & \text{elsewhere,} \end{cases} \tag{3}$$

where ε is a Lennard–Jones well depth and set to $k_{\mathrm{B}}\mathrm{T}$, and $r_{\mathrm{c}} = 2^{1/6}\sigma$. Bonded segments in a chromosome interact with a combination of finite extension nonlinear elastic (FENE) potential

$$U_{\mathrm{b}}(r) = -\tfrac{1}{2}k_{\mathrm{b}}R_{\mathrm{b}}^2 \ln[1-(r/R_{\mathrm{b}})^2] \tag{4}$$

and the repulsive Lennard–Jones potential given in (3). In (4), $k_{\mathrm{b}} = 30k_{\mathrm{B}}\mathrm{T}/\sigma^2$ and $R_{\mathrm{b}} = 1.5\sigma$ to prevent bonds in polymers from crossing each other [24]. The stiffness of the polymer is taken into account by the harmonic angle potential for an angle θ formed by consecutive three segments:

$$U_\theta(r) = \tfrac{1}{2}k_\theta(\theta-\theta_0)^2, \tag{5}$$

where $k_\theta = 4k_{\mathrm{B}}\mathrm{T}$ and $\theta_0 = \pi$. For the given k_θ, the persistence length is calculated to be 120 nm.

The disorder strength L_d, defined in (1), is obtained by calculating density variations $\langle\Delta\rho^2\rangle$ and its correlation length l_{c} in the model nucleus. For their calculation, the cubic simulation box is divided into subcells of $\Delta x \times \Delta y \times \Delta z$. Since the minimum length scale in the model is σ as defined by the diameter of chromosome segments, we vary $\Delta x = \Delta y$ between 2σ and 8σ corresponding to $\Delta x = \Delta y = 60$–240 nm. However, Δz is fixed as σ (= 30 nm) so that the density–density correlation function in the z direction is calculated at more frequent intervals. We have confirmed that qualitative conclusions on the disorder strength do not change when it is calculated for subcells with different $\Delta x = \Delta y$ and Δz.

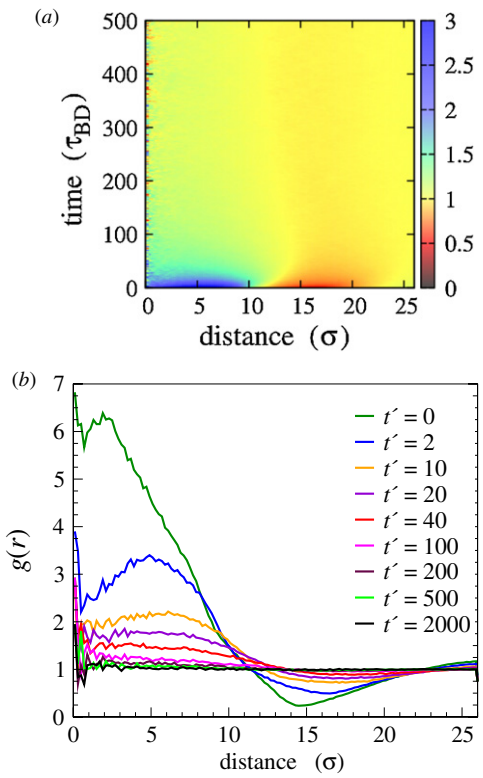

Figure 2. Radial chromosome density function, $g(r)$, averaged over eight chromosomes. The abscissa is a distance from the center of mass of each chromosome. (*a*) Time evolution of radial density function for $t < 500\ \tau_{BD}$. The ordinate is the simulation time in the unit of τ_{BD}. (*b*) Radial density function at specific simulation times, $t' = t/\tau_{BD}$.

4. Results and discussions

Figure 1 shows chromosome conformations in a representative model nucleus during the course of decondensation. Eight chromosomes in the nucleus are colored differently and some parts of the same chromosomes are sometimes shown simultaneously at different corners due to the use of a periodic boundary condition. Initially, the highly compact cylindrical chromosomes are located in the simulation box, occupying 10% of total nuclear volume. There exists a large empty space between highly condensed chromosomes. As simulations proceed, the compact chromosomes start to decondense to increase the polymer conformational entropy and to reduce the excluded volume interactions between chromosome segments. With decondensation, the empty space between chromosomes is reduced and the chromosome densities are delocalized. Since the influence of chromosome condensation is of interest, the nuclear configurations at different times during decondensation in figure 1 are assumed to be those with different chromosome condensation induced by carcinogenesis.

An average radial density function around individual chromosomes is calculated in the course of decondensation and plotted in figure 2 to understand the nuclear density variations with time. Figure 2(*a*) shows the time evolution of the average density variation of total chromosomes. At short times, the chromosome density is very high within a distance of 10σ from a chromosome center around which the radial density function is calculated. The radial density function is close to unity beyond 20σ due to the presence of neighboring chromosomes and is very low in the intermediate region reflecting the empty space between chromosomes. The radial density function becomes more homogeneous with time, and after about $200\ \tau_{BD}$ the spatial inhomogeneity becomes rarely noticeable. The radial density function is shown for specific times in figure 2(*b*). The density inhomogeneity in a cell nucleus becomes less significant after $100\ \tau_{BD}$ and reaches a steady state after $200\ \tau_{BD}$, which is also clear from the snapshots in figure 1.

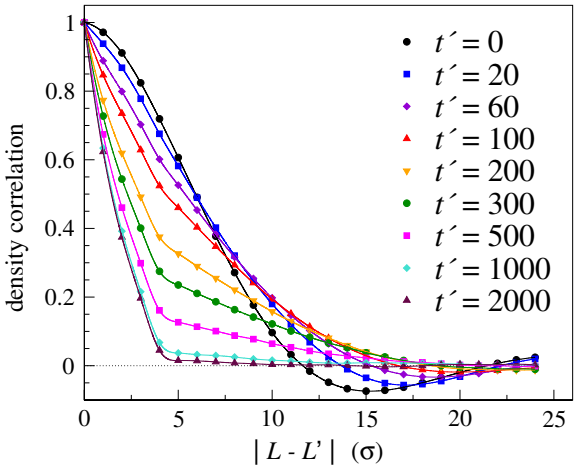

Figure 3. Normalized density correlation function, $\langle \Delta\rho(L)\Delta\rho(L')\rangle / \langle \Delta\rho^2\rangle$, where $\Delta\rho(z) = \langle\rho\rangle - \rho(z)$ and $\langle\rho\rangle$ and $\rho(z)$ are the average chromosome density and the density at z, respectively. The unit of length $\sigma = 30$ nm. In legends, $t' = t/\tau_{BD}$.

For nuclear configurations with different chromosome condensation, average density variation and the density correlation length are calculated, and the disorder strength is calculated from (1). While calculation of the average density variation as $\langle \Delta\rho^2\rangle$ is straightforward, calculation of the density–density correlation length l_c needs a brief discussion. As shown in figure 3, density correlation functions defined as $\langle \Delta\rho(L)\Delta\rho(L')\rangle$ are not exactly exponential functions (L and L' are positions in the z direction along which the correlation function is calculated). In this work, however, we define a correlation length as a length for which the correlation function decays to a value of $1/e$ and use it as a measure to differentiate the density correlation calculated for different degrees of chromosome condensation. This is consistent with the way the correlation length is calculated in the previous paper to analyze the experimental observations [3], and we had also verified that the correlation length defined in different ways does not affect the qualitative conclusions from our simulation studies.

Figure 4 shows the average density variation $\langle \Delta\rho^2\rangle$, the correlation length l_c and the disorder strength L_d as a function of decondensation time (normalized to a corresponding saturation value at $t = 2000\ \tau_{BD}$). Both the average density variation and the correlation length change with chromosome condensation, as well as the disorder strength. To calculate

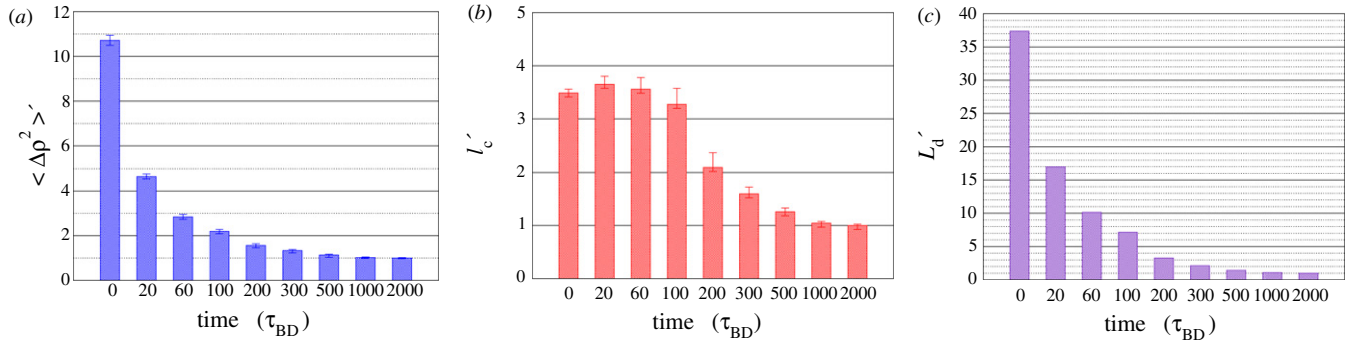

Figure 4. (*a*) Density variations $\langle \Delta\rho^2 \rangle$, (*b*) density correlation length l_c and (*c*) disorder strength L_d for $t = 0$–$2000\ \tau_{BD}$. Each variable at a time (t) is normalized by its corresponding value at $t = 2000\ \tau_{BD}$. The data are calculated when the grid length of subcells is 120 nm in the x and y directions and 30 nm in the z direction.

these quantities the model nucleus is divided into subcells of $\Delta x \times \Delta y \times \Delta z$. Quantitative results depend on the size of subcells, but the qualitative conclusions on the disorder strength do not change with a choice of the subcell size when varied between 60 and 240 nm for $\Delta x = \Delta y$ and between 30 and 60 nm for Δz. The results in figure 4 are calculated for the subcell size of 120 nm × 120 nm × 30 nm.

The disorder strength in figure 4(*c*) is higher when the nuclear density is highly inhomogeneous (i.e. heterogeneous) as can be seen at $t = 0\ \tau_{BD}$ and $20\ \tau_{BD}$, and decreases for a cell nucleus with less condensed chromosomes or for more homogeneous nuclear density. The disorder strength no longer changes after $t = 1000\ \tau_{BD}$. Interestingly, the disorder strength still changes to a non-negligible extent even when the chromosome density distribution is fairly homogeneous after $100\ \tau_{BD}$ as shown in figure 2. This suggests that the disorder strength is highly dependent on the small difference in the degree of chromosome condensation or the minute change of spatial density inhomogeneity.

Although the presence of chromosome territories has been known from experimental observations, it is not clear how much intermingling and mixing occurs between neighboring chromosomes. Current experimental techniques cannot decide the chromosome structures precisely and which configuration in figure 1 resembles the interphase nuclear chromosomes in normal cells. Rosa and Everaers [16] showed that decondensing model chromosomes of 20 Mbp at different times of decondensation result in the mean squared intrachromosome distance consistent with experimental fluorescence *in situ* hybridization (FISH) data. Therefore, simulation results of the model nucleus in this work should be interpreted with an emphasis on the change of a disorder strength caused by a difference in chromosome condensation, not on the absolute value of the disorder strength.

In conclusion, the disorder strength calculated in our model nucleus increases to a significant extent when the chromosomes in the nucleus are slightly more condensed. For instance, the disorder strength increases with chromosome condensation from configurations at time $t = 500\ \tau_{BD}$ to those at $t = 100\ \tau_{BD}$ in figure 1. Using PWS, it was shown that the disorder strength is increased in the earliest stages of carcinogenesis even when the affected cell cannot be distinguished from a normal cell based on its histological appearance [3, 4]. The change in the disorder strength was most pronounced in the cell nucleus [3, 5], and the nuclear density variations by heterochromatin aggregation in late stages have been hypothesized for many types of cancer [1]. Taken together, these results suggest that there can be minute nuclear density variations by structural alterations of chromosomes in a cell nucleus in early carcinogenesis: too subtle structural alterations to be observed in the conventional histological methods, but large enough to be detected by PWS.

5. Conclusions and outlook

PWS measurements in several types of cancerous cells showed the increase of disorder strength with carcinogenesis [3, 4]. In this work we investigated the effect of chromosome condensation on the change of disorder strength by computer simulations, in order to appreciate the contribution of chromosome condensation to the disorder strength observed in PWS measurements.

The decondensation of highly compact chromosomes driven by polymer conformational entropy and excluded volume interactions was simulated. A model nucleus at different times of decondensation is assumed to have similar chromosome distributions to those of biological cells during carcinogenesis. The disorder strength calculated for different nuclear configurations increases for those with more condensed chromosomes. The disorder strength reached a steady state when the chromosome density becomes homogeneous in the entire nucleus. We conclude that the disorder strength increases significantly even for the minute changes of chromosome condensation and the resulting spatial inhomogeneity. Coupled with PWS measurements, our simulation study suggests that there can be nuclear density variations by chromosome condensation in a cell nucleus in early stages of carcinogenesis.

The chromosome model used in this work is a simplistic model devised to correlate the different degrees of chromosome condensation with changes in density variations and its correlation length. The minimum and maximum of correlation lengths calculated in this model (i.e. 60 and

210 nm) are largely determined by scales of chromosome segments ($\sigma = 30$ nm) and initial compact chromosomes (∼200 nm), respectively. Further study would incorporate the full range of the correlation length by using more detailed model of chromosomes composed of nucleosomes and with the realistic length on the order of about 100 Mbp. In addition, other nuclear structures such as nucleoli and cajal bodies could make a significant contribution to the local increase of disorder strength observed in carcinogenesis. The study of density variations by these nuclear structures would also represent possible future directions of this work.

Little is known about the mechanism of chromosome condensation. One of the hypotheses is the modification in activities of proteins mediating the chromosome binding and looping. When the protein-mediated binding between chromatin fibers becomes stronger or more frequent, the chromosome structure can become more condensed. Another hypothesis is the environmental change in a cell nucleus such as increased concentration of non-histone proteins by overexpression or nuclear volume change. The chromosome compaction by the increased macromolecular concentration was proven by osmotically induced crowding [26, 27]. These two hypotheses represent our research directions, and currently efforts are being made to understand the nuclear environment and its influence on nuclear nanoarchitecture in more detail.

Acknowledgments

This work is supported by the National Science Foundation under grant EFRI CBET-0937987. We thank Hariharan Subramanian and Jennifer Campbel for carefully reading the manuscript.

References

[1] Zink D, Fischer A H and Nickerson J A 2004 Nuclear structure in cancer cells *Nat. Rev. Cancer* **4** 677–87
[2] Meaburn K J, Gudla P R, Khan S, Lockett S J and Misteli T 2009 Disease-specific gene repositioning in breast cancer *J. Cell Biol.* **187** 801–12
[3] Subramanian H *et al* 2008 Optical methodology for detecting histologically unapparent nanoscale consequences of genetic alterations in biological cells *Proc. Natl Acad. Sci. USA* **105** 20118–23
[4] Subramanian H *et al* 2009 Nanoscale cellular changes in field carcinogenesis detected by partial wave spectroscopy *Cancer Res.* **69** 5357–63
[5] Pradhan P, Damania D, Joshi H, Turzhitsky V, Subramanian H, Roy H K, Taflove A, Dravid V and Backman V 2011 Quantification of nanoscale density fluctuations by electron microscopy: probing cellular alterations in early carcinogenesis *Phys. Biol.* at press
[6] Sachs R K, van den Engh G, Trask B, Yokota H and Hearst J E 1995 A random walk/giant-loop model for interphase chromosomes *Proc. Natl Acad. Sci. USA* **92** 2710–4
[7] Croft J A, Bridger J M, Boyle S, Perry P, Teague P and Bickmore W A 1999 Differences in the localization and morphology of chromosomes in the human nucleus *J. Cell Biol.* **145** 1119–31
[8] Cremer T and Cremer C 2001 Chromosome territories, nuclear architecture and gene regulation in mammalian cells *Nat. Rev. Genet.* **2** 292–301
[9] Dekker J, Rippe K, Dekker M and Kleckner N 2002 Capturing chromosome conformation *Science* **295** 1306–11
[10] Dostie J *et al* 2006 Chromosome conformation capture carbon copy (5C): a massively parallel solution for mapping interactions between genomic elements *Genome Res.* **16** 1299–309
[11] Lieberman-Aiden E *et al* 2009 Comprehensive mapping of long-range interactions reveals folding principles of the human genome *Science* **326** 289–93
[12] Misteli T 2004 Spatial positioning: a new dimension in genome function *Cell* **119** 153–6
[13] Meaburn K J and Misteli T 2007 Chromosome territories *Nature* **445** 379–81
[14] Münkel C, Eils R, Dietzel S, Zink D, Mehring C, Wedemann G, Cremer T and Langowski J 1999 Compartmentalization of interphase chromosomes observed in simulation and experiment *J. Mol. Biol.* **285** 1053–65
[15] Mateos-Langerak J *et al* 2009 Spatially confined folding of chromatin in the interphase nucleus *Proc. Natl Acad. Sci. USA* **106** 3812–7
[16] Rosa A and Everaers R 2008 Structure and dynamics of interphase chromosomes *PLoS Comput. Biol.* **4** e1000153
[17] Grosberg A, Rabin Y, Havlin S and Neer A 1993 Crumpled globule model of the three dimensional structure of DNA *Europhys. Lett.* **23** 373–8
[18] Rosa A, Becker N B and Everaers R 2010 Looping probabilities in model interphase chromosomes *Biophys. J.* **98** 2410–9
[19] Barer R, Ross K F A and Tkaczyk S 1953 Refractometry of living cells *Nature* **171** 720–4
[20] Davies H G and Wilkins M H F 1952 Interference microscopy and mass determination *Nature* **169** 541
[21] Tremethick D J 2007 Higher-order structures of chromatin: the elusive 30 nm fiber *Cell* **128** 651–4
[22] Ermak D L and McCammon J A 1978 Brownian dynamics with hydrodynamic interactions *J. Chem. Phys.* **69** 1352–60
[23] van der Spoel D, Lindahl E, Hess B, Groenhof G, Mark A E and Berendsen H J C 2005 GROMACS: fast, flexible and free *J. Comput. Chem.* **26** 1701–18
[24] Kremer K and Grest G S 1990 Dynamics of entangled linear polymer melts: a molecular-dynamics simulation *J. Chem. Phys.* **92** 5057–86
[25] Humphrey W, Dalke A and Schulten K 1996 VMD: visual molecular dynamics *J. Molec. Graph.* **14** 33–8
[26] Richter K, Nessling M and Lichter P 2007 Experimental evidence for the influence of molecular crowding on nuclear architecture *J. Cell Sci.* **120** 1673–80
[27] Albiez H *et al* 2006 Chromatin domains and the interchromatin compartment form structurally defined and functionally interacting nuclear networks *Chromosome Res.* **14** 707–33